Proceedings of the ASME 2024 International Design Engineering Technical Conferences & Computers and Information in Engineering Conference
IDETC/CIE 2024
August 25-28, 2024, Washington, DC, USA

DETC2024-143347

CFD-DRIVEN TOPOLOGY OPTIMIZATION FOR PERSONALIZED INTRACRANIAL ANEURYSM IMPLANT DESIGN

Weijun Lei
Department of Mechanical Engineering
State University of New York at Stony Brook
Stony Brook, NY 11794, USA
Email: weijun.lei@stonybrook.edu

Chander Sadasivan
Department of Neurological Surgery
Stony Brook University Medical Center
Stony Brook, NY 11794, USA
Email:csadasivan@sbumed.org

Xianfeng David Gu
Department of Computer Science
Department of Applied Mathematics and Statistics
State University of New York at Stony Brook
Stony Brook, NY 11794, USA
Email: gu@cs.stonybrook.edu

Shikui Chen*
Department of Mechanical Engineering
State University of New York at Stony Brook
Stony Brook, NY 11794, USA
Email: shikui.chen@stonybrook.edu

ABSTRACT

Intracranial aneurysm rupture causes life-threatening subarachnoid hemorrhage. Current endovascular devices like coils, flow diverters, and intravascular implants aim to thrombose the aneurysm but have limitations and varying success rates depending on aneurysm characteristics. We propose a new computational framework integrating CFD and topology optimization to design personalized aneurysm implants. The optimization problem aims to reduce blood flow velocity within the aneurysm while ensuring adequate structural integrity of the implant. The fluid dynamics are governed by the Navier-Stokes equations, while the solid mechanics are described by the linear elasticity equations. A Darcy-Brinkman model is employed to simulate flow through the porous implant in the fluid domain, while the Solid Isotropic Material with Penalization (SIMP) method is used to interpolate between solid and void regions in the structural domain during topology optimization. The objective combines fluid energy dissipation ratio and solid strain energy with spatially varying weights. Global and local volume constraints generate personalized implants with porosity and flow-diverting architectures. The approach is demonstrated on patient-specific aneurysm geometries from rotational angiography. This CFD-driven topology optimization method enables personalized aneurysm implant design to potentially improve occlusion rates and reduce complications compared to current devices. Further studies will validate the optimized designs and investigate their efficacy in vitro and in vivo.

Keywords

Aneurysm. Personalized aneurysm implants. Topology optimization. Porous structure. Power dissipation.

1 INTRODUCTION

Subarachnoid hemorrhages (SAH) are life-threatening and result from the accumulation of blood between the arachnoid and pia mater. SAH incidence ranges from 10 to 14 cases per 100,000 individuals annually [1]. Aneurysms are focal pouch-like dilations of the cerebral vasculature that have a weak wall that can

*Address all correspondence to this author.

rupture. The anatomy of aneurysms and associated parent vessels can be highly complex and show substantial variability from patient to patient (Figure1). Aneurysm rupture is the cause of subarachnoid hemorrhage in 85% of cases. The case fatality after aneurysmal hemorrhage is 50%; one in eight patients with subarachnoid hemorrhage dies outside the hospital [2]. Most aneurysms are currently treated by endovascular methods. The goal for all endovascular treatment is to reduce flow velocities within the aneurysm sac to induce intra-aneurysmal thrombus formation. Over weeks to months, this thrombus undergoes organization to fibrous scar tissue, and the aneurysmal structure is eventually resorbed as much as possible with permanent implants inside the sac. A similar response occurs at the aneurysm neck-device interface, resulting in the formation of a stable endothelialized neointimal layer on the device [3–6]. When this endothelialization is complete, the aneurysm is considered to be successfully treated. There are three predominant device types currently used for endovascular treatment (Figure2) – coiling (metallic micro-coils fill the aneurysm), flow diversion (fine-mesh metallic stent implanted in parent vessel), and intravascular implants ("ball"-shaped metallic mesh implanted inside the aneurysm) – all of which have successful outcomes in 70-80% of cases on average.

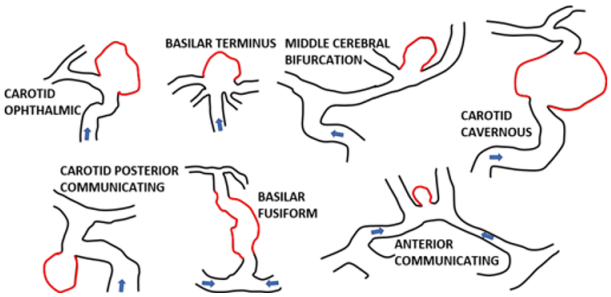

FIGURE 1. VARIOUS LOCATIONS AND SHAPES/DIMENSIONS OF BRAIN ANEURYSMS (RED LINES). ARROWS SHOW THE DIRECTION OF FLOW OR PROXIMAL TO DISTAL ENDOVASCULAR APPROACH

However, success rates with these devices are highly dependent on the location and type of aneurysm. Effective coiling is technically challenging in aneurysms with complex and wide-necked geometries [9]. Flow diversion can be ineffective in 35-50% of aneurysms because they arise at bifurcations [10]. Furthermore, the aftermath of initial treatment using coil embolization is fraught with substantial challenges, including parent artery obstruction, collapsed coils, coil malposition, and, notably, the potential for coil migration [11]. These issues underscore the need for innovative approaches to enhance the efficacy and safety of this widely employed technique. The deployment of flow diverters and intravascular flow disruptors presents an alternative method. The complexity of achieving effective blood flow diversion necessitates the design of multi-segment diverters, each tailored according to computational fluid dynamics (CFD) [12]. Patients treated with flow diverters also have to be put on dual antiplatelet medication (aspirin plus clopidogrel) to avoid in-stent thrombosis and thromboembolic ischemia. The primary drawback of intravascular implants is related to sizing and conformability, i.e., they cannot conform to irregular aneurysm shapes and have poor outcomes in larger aneurysms and aneurysms with unfavorable aspect ratios (ratio of height to the neck). A systematic review showed a pooled complication rate of 12% with complete aneurysm occlusion rates of 58% and residual neck of 28% at final follow-up (13±10 months), with retreatment required in 7% of the cases [13].

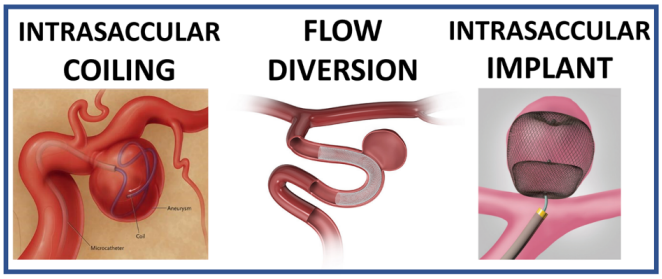

FIGURE 2. EXAMPLES OF ENDOVASCULAR DEVICES TO TREAT BRAIN ANEURYSMS. (TOP ROW) INTRAVASCULAR COILING, INTRAVASCULAR FLOW DIVERSION, AND INTRAVASCULAR IMPLANTS. FROM ONLINE [7, 8]

Overall, several devices are being used to treat aneurysms, and different device types are being developed to treat different classes of aneurysms. Limitations and complications remain, and no single device is currently available that can safely and reliably treat all classes of aneurysms.

Computational Fluid Dynamics (CFD) stands as a potent computational technique employed for simulating fluid flow and comprehending its behavior within intricate geometries. Over an extended period, CFD has proven invaluable in discerning mechanical risk factors linked to aneurysmal evolution and rupture. It also aids in unraveling flow characteristics pre- and post-surgical interventions, contributing to informed clinical decision-making processes [14, 15]. Rupture risk assessment in aneurysms can be effectively evaluated through parameters such as shear stress, fluid pressure, relative residence time, and non-dimensional inflow rate [16]. However, the explicit incorporation of coil geometry into CFD simulations, a critical aspect in assessing the postoperative risk of inducing new arterial aneurysms, poses challenges. Some researchers have explored coil models represented by porous models, demonstrating mean velocity in the aneurysmal sac comparable to coil-resolved models [12, 17]. Coil design, typically tailored to the aneurysm's shape, involves

considerations of coil shape, orientation, and thickness within a relatively constrained design space. This intricate process, guided by the experience of medical professionals, underscores the complex nature of coil design [18–20]. The intricacies of designing coils that balance navigational precision and shape adjustability represent pressing areas necessitating dedicated research efforts. Topology optimization emerges as a promising solution to delve deeper into the design space and achieve a high-performance or patient-specific implant design.

Topology optimization is a technique to find the optimal shape and material distribution of a structure under certain constraints and objectives. It can be used to design lightweight, stiff, and efficient structures for various applications. The homogenization approach to topology optimization was proposed by Bendsoe and Kikuchi in 1988 [21]. A number of different methods are developed based on the homogenization approach such as the artificial density method(Bendsoe; Zhou and Rozvany; Mlejnek [22–24]); level set methods (Allaire et, Wang [25,26]); evolutionary approaches (Xie and Steven [27]) and several others. The Level Set Method is an implicit approach that incorporates the zero-level contour and negative and positive values within the level set function, distinctly representing structural boundaries, voids, and solids in the design domain. Due to its ability to provide clear boundaries, this method is well-suited for structural design in fluid fields. Duan et al. were the first to apply a variational level set method for solving Navier–Stokes flow topology optimization [28–30]. Zhang uses the level set method on arterial bypass configurations, demonstrating its potential applicability in the design of medical devices [31]. However, its utilization in 3D structure design faces challenges, primarily stemming from the high computational costs and space variable complexities associated with this method.

The Solid Isotropic Material with Penalization (SIMP) approach is another significant classical method that makes it easy to generate the structure. A physical justification of SIMP was provided in Bendsøe and Sigmund [32]. Its incorporation into fluid topology optimization dates back to the early 21st century, marking a pivotal development in the field. The seminal paper by Borrvall and Petersson first solved the topology optimization problems for fluid systems [33]. This method has also found application in medical research related to cardiovascular stents [34, 35].

While CFD has been widely used to characterize aneurysm flow dynamics and virtualize treatment [14, 36–38] , topology optimization based on CFD-derived hemodynamics remains unexplored for aneurysm implant design. Prior studies have used CFD to assess coil packing density and flow diversion effects [39–41] and optimize coil shape and orientation [18, 42, 43] . However, these studies focus on conventional coil designs within a limited design space. Jiang et al. [44] applied topology optimization to aneurysm treatment using simplified models but did not consider patient-specific hemodynamics or clinically relevant design constraints Sá et al. performed multi-objective optimization on a small-scale pump, aiming to minimize energy dissipation and vorticity which is also suitable for the blood flow problem in aneurysm [45].

Our approach expands the implant design space beyond conventional devices to generate hemodynamically optimized and patient-specific designs. By integrating CFD-derived hemodynamic objectives and constraints related to deliverability and structural integrity, we enable the design of implants featuring a shell structure endowed with porosity, incorporating a sizable void within and flow-diverting microarchitectures. This paves the way for personalized aneurysm treatment with the potential to improve occlusion rates and reduce complications compared to current devices.

This paper is structured as follows: Section. 2 outlines the problem formulation and modeling. Section. 3 details the extraction of patient data, the setup of the topology optimization problem, and optimal implant results. Section. 4 focuses on conclusion and future work.

2 TOPOLOGY OPTIMIZATION OF PERSONALIZED ANEURYSM IMPLANTS

2.1 Topology optimization objective function formulation

This paper aims to design an implant for arterial aneurysms with the primary objectives of reducing the dwell time of blood within the aneurysm and slowing down the blood flow velocity. The implant is intended to provide both structural support and guidance for the placement of the implant. To facilitate the reader's understanding of the problem, a schematic representation of the problem setup is illustrated in Figure3.

There are two governing equations within the design domain: The Navier-Stokes equation, describing fluid dynamics; and the Cauchy momentum equation, describing linear elasticity:

$$\begin{aligned} &\rho \frac{\mathrm{D}\mathbf{v}}{\mathrm{D}t} = -\nabla p + \mu \nabla^2 \mathbf{v} + \mathbf{f} \\ &\nabla \cdot \mathbf{v} = 0 \\ &v = v_{in}, \ \ on \ \ \Gamma_{in} \\ &p = 0, \ \ on \ \ \Gamma_{out} \end{aligned} \tag{1a}$$

$$\begin{aligned} &\nabla \cdot \sigma + \mathbf{F} = \rho \ddot{\mathbf{u}} \\ &u = 0, \ \ on \ \ \Gamma_D \\ &p = p_b, \ \ on \ \ \Gamma_N \end{aligned} \tag{1b}$$

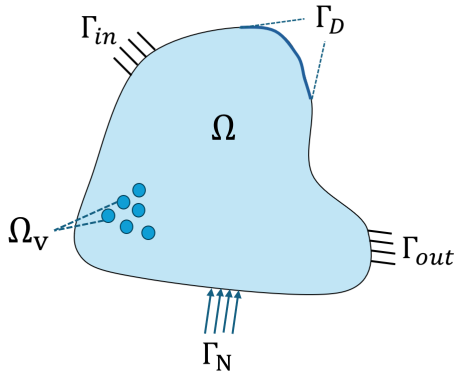

FIGURE 3. SCHEMATIC DIAGRAM FOR THE ANEURYSM MODEL SETTING

Equation (1a) refers Navier-Stokes equations for an incompressible fluid; Equation (1b) refers the liner elastic equation.

The region denoted by Ω represents the area of the arterial aneurysm, serving as the design domain. Ω_v is a subset of Ω, meaning local constraints domain. Γ_{in} and Γ_{out} are Robin boundary conditions(BCs) which symbolize the inflowing and ouflowing blood area. There are various selections for these conditions, and this study specifies velocity $v = v_{in}$ as the inflow condition and pressure $p = 0$ as the outflow condition. This configuration has been chosen to enhance the stability of numerical solutions and facilitate their coupling with the energy equation, which is the objective function of the optimization problem. Dirichlet boundary condition Γ_D is applied with $u = 0$ and Neumann boundary condition $p = p_b$ on Γ_N means the external pressure which is equal to the blood pressure in the aneurysm.

The objective function for the implant can be formulated as follows:

$$\begin{aligned} Obj &= \omega_1 \cdot Obj\_fluid + \omega_2 \cdot Obj\_solid \\ \omega_1 &= \frac{1}{1 \times 10^{\mathscr{O}(Obj\_fluid_i)-1}} \\ \omega_2 &= \frac{1}{1 \times 10^{\mathscr{O}(Obj\_solid_j)}} \end{aligned} \tag{2}$$

Where ω_1 and ω_2 represent the corresponding weights assigned to each sub-objective function, while $\mathscr{O}$ reflects the magnitude on the order of scale specific to these functions. The indices i and j determine the values taken in the sub-objective function for the specified iteration. In this paper, i and j are set to 10.

In Figure1, the problem is formulated based on the physical fields existing in a real patient's aneurysm with forward blood flow. To achieve a robust design, a virtual reverse flow is proposed to optimize the structure and prevent the connection between the aneurysm and the blood vessel. Simultaneously, this helps to reduce the dwell time of blood within the aneurysm, given that blood tends to flow out easily but encounters difficulty in this area. For the reverse flow, all governing equations remain unchanged. The BCs as the inlet and outlet are swapped as follows:

$$\begin{aligned} p_I &= 0, \ \ on \ \ \Gamma_{in} \\ v_I &= v_{out}, \ \ on \ \ \Gamma_{out} \end{aligned} \tag{3}$$

where v_{out} represents the outlet velocity on Γ_{out} computed from forward flow.

Based on these, the fluidic optimization objective function can be formulated as the ratio between the forward fluid energy dissipation and the inverse fluid energy dissipation like:

$$\begin{aligned} \text{Minimize: } Obj\_fluid &= \left(\frac{\Phi_I + \phi_I}{\Phi_f + \phi_f} \right)^2 \\ \Phi &= \int_\Omega \tau{:}(\nabla \mathbf{v}) \, dV \\ \phi &= \int_\Omega \alpha(\mathbf{v} \cdot \mathbf{v}) \, dV \end{aligned} \tag{4}$$

where index f and I refer to the forward direction and reverse direction. Ω is the aneurysm domain. Φ is the viscosity dissipation and ϕ is the body force friction dissipation.

As we stated before, the implant needs to be supportive and directive, and objective function can be described as a mean compliance problem:

$$\text{Minimize: } Obj\_solid = \int_\Omega \left(\varepsilon^T \mathbf{E} \varepsilon \right) \, dV \tag{5}$$

where $\mathbf{E}$ is the stiffness matrix. $\varepsilon^T \mathbf{E} \varepsilon$ is the strain energy density.

The boundary conditions on Γ_D and Γ_N in the linear elasticity governing equation assist in achieving the design of an implant with implantation guidance. Furthermore, this implant exhibits a specific load strength and a continuous structure, allowing it to exert a long-term effective impact on the aneurysm region.

2.2 Artificial density material

The structural design of implants within an arterial aneurysm can be simulated by introducing a virtual artificial density. The material in the fluid region is considered a porous structure, where regions approaching solid indicate finer porosity. The

boundary between fluid and approaching solid is treated as a no-slip boundary, implying that as the area of contact with the solid increases, so does the frictional force. Therefore, volume forces can be utilized to distinguish between solid and liquid regions. Darcy's law, a well-established method, defines fluid flow through porous media. It states that the fluid flow per unit area and pressure drop per unit length are proportional and inversely proportional to the resistance posed by the porous medium to the flow [33,46]. In this paper, this relationship can be expressed as follows:

$$\begin{aligned} f &= -\alpha \mathbf{v} \\ \alpha &= 10^7 \frac{1-\gamma}{0.05+\gamma} \end{aligned} \tag{6}$$

where f is the body force.

To distinguish between the solid and fluid domains in the linear elastic governing equations, a power-law penalization approach is employed for formulation as follows:

$$E = (1-\gamma^n)\cdot E_1 + \gamma^n \cdot E_2 \tag{7}$$

where the penalization factor is selected to be 3. E_1 and E_2 are $1.35MPa$ and $1Pa$.

The parameter γ serves as a virtual artificial density, exhibiting variation within the range of 0 to 1. Specifically, γ signifies the fluid domain when approaching 1, and conversely, it indicates the structural domain when approaching 0. This parameter plays a crucial role in characterizing the transitional nature between the fluid and structural components within the computational model.

2.3 Optimization Constraints

In this study, two types of volume constraints are implemented to provide nuanced control over the optimized structures, specifically aiming to generate a porous structure with internal channels. The first type is characterized by a conventional overall volume constraint. The second type introduces a set of distributed local volume constraints within the neighborhood of a specified radius. To achieve this, an artificial array of 4x4x4 local positions is defined within the aneurysm domain. Within each of these defined positions, a local volume constraint is articulated within a neighborhood radius of $0.45mm$ [44,47]. It's applied:

$$\begin{aligned} &0.15 < \frac{\int_\Omega (1-\gamma)\, dV}{\int_\Omega 1\, dV} < 0.2 \\ &0.15 < \frac{\int_{\Omega_n} (1-\gamma)\, dV}{\int_{\Omega_n} 1\, dV} < 0.2 \\ &\Omega_n \in \Omega_v\ ,\ \ n = 1,\ldots,64 \end{aligned} \tag{8}$$

The incorporation of the Heaviside function is instrumental in selecting and implementing the local constraints due to its suitability for derivation purposes. Ω_n is defined by the Heaviside function, which is a smoothed function with a continuous second derivative without overshoot as:

$$H(x,d) = \begin{cases} 0, & \text{if } x \le -d \\ 1, & \text{if } x \ge d \\ a_1 + a_2\cdot\left(\frac{x}{d}\right) + a_3\cdot\left(\frac{x}{d}\right)^3 + a_4\cdot\left(\frac{x}{d}\right)^5, & \text{otherwise} \end{cases} \tag{9}$$

$$S_n = 1 - H\left(r_n - R, 0.05\times 10^{-3}\right)\ ,\ \ S_n \text{ refers to } \Omega_n \tag{10}$$

where $a_1 = 0.5$, $a_2 = 0.9375$, $a_3 = -0.625$, $a_4 = 0.1875$, $R = 0.45mm$. r is the distance to local constraint centers. The local constraints are chosen as table 1.

TABLE 1. LOCAL CONSTRAINTS CENTER COORDINATES(MM)

X	-0.4	0.4	1.2	2.0
Y	-0.5	-1.3	-2.1	-2.9
Z	0.0	0.8	1.6	2.4

This meticulous application of volume constraints enhances the precision of the optimization process and introduces localized features within the porous structure, contributing to its overall design intricacy.

Hence, the entire topology optimization problem can be expressed in the following form:

$$\begin{aligned} Minimize: &\quad Obj = \omega_1 \cdot Obj\_fluid + \omega_2 \cdot Obj\_solid \\ s.t: &\quad 0.15 < \frac{\int_\Omega (1-\gamma)\, dV}{\int_\Omega 1\, dV} < 0.2 \\ &\quad 0.15 < \frac{\int_{\Omega_n} (1-\gamma)\, dV}{\int_{\Omega_n} 1\, dV} < 0.2 \\ &\quad \Omega_n \in \Omega_v\ ,\ \ n = 1,\ldots,64 \end{aligned} \tag{11}$$

3 NUMERICAL EXAMPLE

3.1 3D geometry reconstruction

The data utilized in this study are sourced from authentic patient records. Pre-treatment rotational angiography scans of brain aneurysm patients were retrospectively and anonymously collected under Institutional Review Board approval. The aneurysm

models were extracted from instances located at the bifurcation of cerebral blood vessels. Axial slices from the rotational angiograms were imported into 3D Slicer (slicer.org), segmented using global thresholding, and the aneurysm geometry was exported as an STL file as outlined in Figure 4.

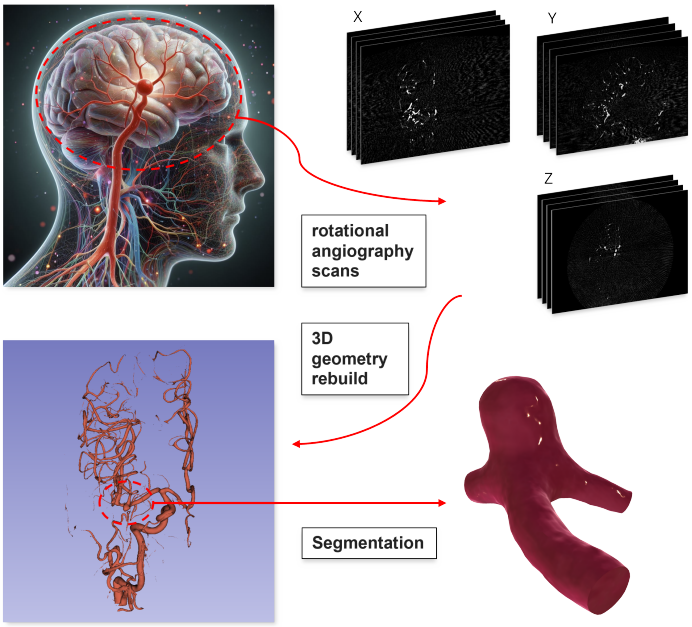

FIGURE 4. PRE-TREATMENT IMAGES SEGMENTATION PROCESS

3.2 Boundary Conditions Parameters Setting

In establishing the boundary conditions, fluid flow is assumed as an incompressible laminar flow with a Reynolds number of 500. The density and viscosity of the fluid are respectively set to $1.1 \times kg/m^3$, $3.5 \times 10^3 Pa \cdot s$. The inflow velocity of forward flow is determined in accordance with the specified Reynolds number, while the inflow velocity of the reverse virtual fluid is assigned an average outflow velocity derived from the computations for forward flow. All boundaries are enforced as no-slip conditions. On the solid front, Dirichlet boundary conditions are rigorously imposed at the neck of the vessel where the aneurysm connects to the blood vessel. Furthermore, a virtual uniform pressure, equivalent to the blood pressure $(15KPa)$, is applied at the selected surfaces of the aneurysm on Γ_N, as highlighted in Figure 5

3.3 Optimization Results

In this paper, an optimizer is implemented on COMSOL® Multiphysics software with the method of moving asymptotes

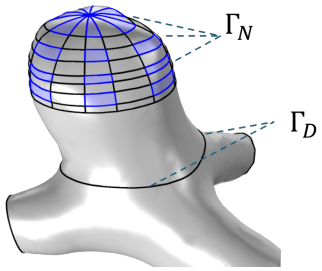

FIGURE 5. SOLID BOUNDARY CONDITION

(MMA). COMSOL has the advantage of managing multiple physics fields effectively, and the implementation of MMA serves as a robust approach to optimize the established model in this research context.

Figure 6 illustrates the correspondence between the model and the original patient geometry, showcasing the structural evolution during the optimization process. Snapshots are taken at the initial state and after the 4th, 10th, 30th, and 80th iterations. Although the overall objective function comprises both fluid and solid components, it is the fluid aspect that predominantly signifies the implant's potential efficacy in treating the aneurysm. Strategic weighting between fluid and solid considerations ensures that the optimization is fluid-centric in the initial 20 iterations. During this phase, as the fluid objective function decreases, the solid objective function experiences an initial increase followed by a subsequent decrease. In the subsequent 60 iterations, the focus shifts primarily to the solid objective function, incorporating overall and local constraints to craft a porous, continuous, and manufacturable structure. The optimal structure

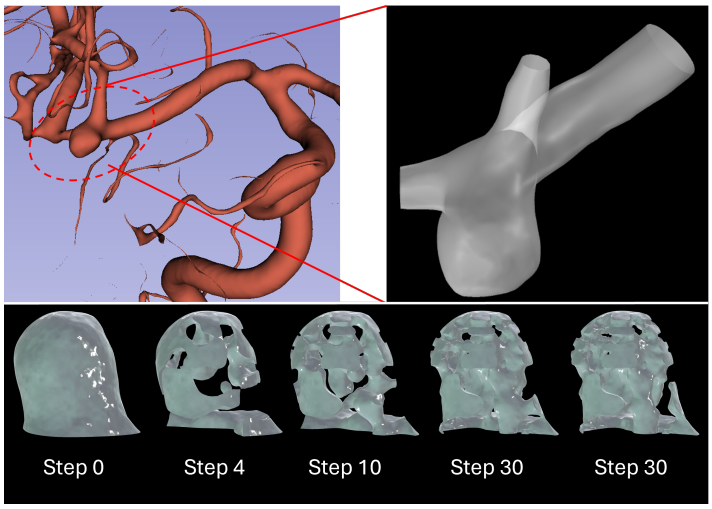

FIGURE 6. TOPOLOGY OPTIMIZATION PROCESS OF THE IMPLANT

is generated with relatively good continuity and porosity as in Figure7. The upper and lower sections of the implanted structure closely resemble the outer wall of the aneurysm and the neck where the aneurysm connects to the blood vessels. This similarity offers valuable guidance during the implantation surgery and minimizes the risk of the aftermath of initial treatment such as collapse and slippage, common occurrences during coil implantation. Additionally, a well-designed porous interconnected structure will be better able to induce intra-aneurysmal thrombus formation.

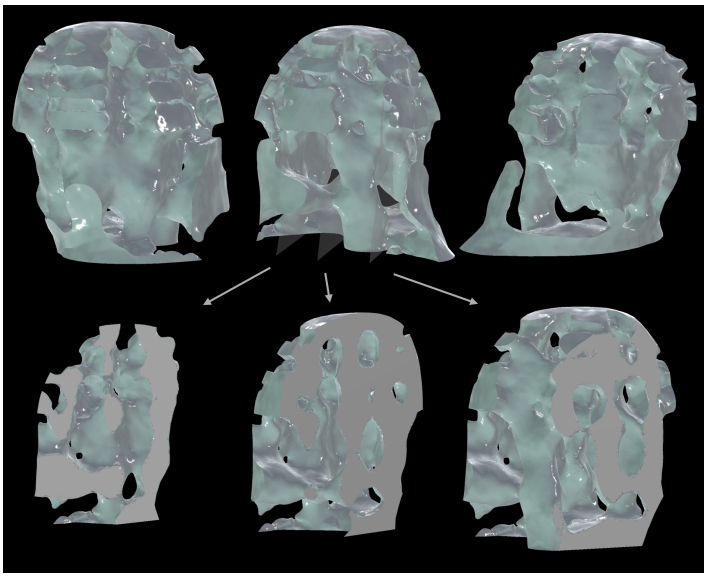

FIGURE 7. IMPLANT STRUCTURE IN MULTI-ANGLES AND MULTI-CROSS SECTIONS

Figure 8 provides visual comparisons of the pre- and post-treatment flow fields, clearly illustrating the reduction in flow velocities and the establishment of more stagnant intra-aneurysmal flow patterns following the implantation of the optimized design. The streamlines in both images start from the inflow domain with a consistent count of 1000 streamlines.

To qualitatively assess the performance of the optimized implant design, we compare key hemodynamic metrics before and after virtual implantation, as summarized in Table 2.

TABLE 2. IMPACT OF THE OPTIMIZED IMPLANT

Metric	Pre	Post	Improv.
Mean velocity (m/s)	0.695	0.157	77.4%
Fluid obj. func.	1.42	0.30	78.9%

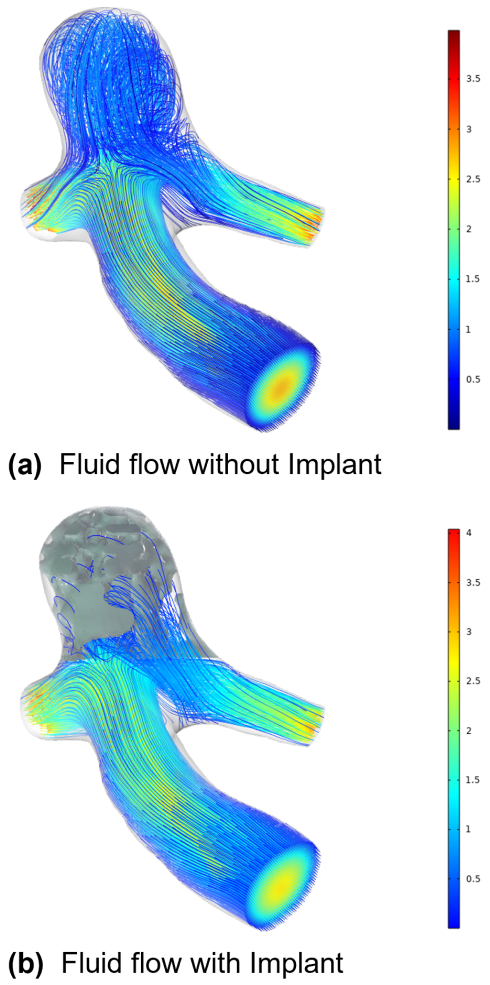

FIGURE 8. FLUID FLOW PERFORMANCE WITH COLOR GRADIENT CORRESPONDING TO THE VELOCITY RANGE

The optimization results demonstrate substantial improvements in the fluid's objective function and intra-aneurysmal flow velocity. The fluid objective function, which represents the ratio between the forward and reverse fluid energy dissipations, decreased from 1.42 to 0.30, indicating a 78.9% improvement in achieving the desired one-way circulation. If the fluid objective function approaches zero, it implies that our structure can achieve nearly complete unidirectional flow. In other words, when the structure is ideally placed, the blood flowing in the forward direction would hardly enter the region of the aneurysm. A 78.9% improvement in the objective function signifies a substantial decrease in the amount of incoming blood. As observed in Figure 8, the streamline diagram illustrates that streamlines face difficulty reaching the depths of the aneurysmal sac, indicating that the implant demonstrates a certain flow diverter effect. Moreover, the mean flow velocity within the aneurysm

sac was reduced by 77%, from $0.69453 m/s$ before treatment to $0.15718 m/s$ after implantation of the optimized design. One of the primary reasons for the recurrence of aneurysms after surgery is the lack of stagnant flow and insufficiently low intra-aneurysmal flow velocity [48]. The reduction in average blood flow velocity significantly contributes to the formation of intravascular thrombus, thereby reducing the risk of postoperative recurrence. These findings underscore the significant impact of the optimized implant on the fluid dynamics within the aneurysm.

4 CONCLUSION AND FUTURE WORK

In this study, we presented a computational framework integrating CFD and topology optimization for the design of personalized intracranial aneurysm implants. The proposed approach addresses the limitations of current endovascular devices by leveraging patient-specific data and an expanded design space to generate optimized porous implants that reduce intra-aneurysmal flow velocity and enhance flow stasis for improved thrombosis.

Key contributions of this work include:

1. A multi-physics topology optimization formulation that couples fluid dynamics, solid mechanics, and porous media flow to design implants that modulate aneurysmal flow while maintaining structural integrity and deliverability.
2. A patient-specific optimization problem that incorporates clinically relevant hemodynamic objectives, local and global porosity constraints, and anisotropic elasticity to enable high-resolution implant design.
3. Demonstration of the framework using real patient anatomies, with optimized implants achieving a 77.4% reduction in mean intra-aneurysmal velocity and a 78.9% improvement in the fluid objective function compared to pre-treatment flows.

The optimized porous architectures achieve significant hemodynamic improvements by diverting flow from the aneurysm neck, reducing inflow velocity, and promoting flow stasis within the aneurysm sac. These improvements are realized through a combination of global and local topology changes that would be difficult to achieve using conventional implant designs. The use of a continuum material interpolation scheme enables the generation of intricate microarchitectures that can enhance flow stasis and thrombosis potential.

The current study has some limitations, including the use of steady flow conditions, idealized boundary conditions, and a limited number of patient anatomies. Future work will focus on extending the framework to unsteady flows, incorporating more physiological boundary conditions, and investigating the effects of non-Newtonian rheology and vessel wall compliance. Rigorous validation studies, including in vitro flow experiments and in vivo animal studies, will be essential to assess the hemodynamic performance, thrombotic potential, and biocompatibility of the optimized implants. Although easy to implement, the SIMP-based method employed in this study tends to introduce intermediate densities, so-called "grey region". Some sophisticated filtering schemes need to be applied to render a crisp "0-1" design. To enhance the stability and robustness of the generated structures, the level set method is another potential topology optimization method to obtain explicit fluid-solid boundaries [49–51].

From a translational perspective, the personalized implants will need to be fabricated using 3D printing or advanced manufacturing techniques and tested for mechanical integrity, durability, and deliverability. A streamlined clinical workflow, from patient imaging to implant design and manufacturing, will need to be developed to enable rapid, on-demand production of patient-specific implants. Therefore, this method is primarily intended for non-ruptured and non-emergent aneurysms or situations where a redesign of the implant is necessary for recurrent aneurysms after initial emergency intervention. Regulatory approval and reimbursement strategies will also need to be established to facilitate clinical adoption.

In conclusion, this study demonstrates the potential of integrating CFD and topology optimization to design personalized aneurysm implants that can significantly improve hemodynamic outcomes compared to current devices. The future deployment of implants through a catheter into the target aneurysm is also a subject that requires improvement and consideration. With further development and validation, this approach may enable a new paradigm of personalized endovascular aneurysm treatment that can reduce complications and improve long-term patient outcomes. The framework presented here can also be extended to other cardiovascular applications where patient-specific implant design is critical, such as coronary stents, transcatheter valves, and vascular grafts.

ACKNOWLEDGMENT

This work was supported in part by the Long Island Network for Clinical Translational Science pilot award, the National Institutes of Health under grant R21EB029733, the National Science Foundation through grants CMMI-1762287 and PFI-RP-2213852, and the Office of the Vice President for Research (OVPR) at Stony Brook University through the Summer 2022 and Fall 2023 Seed Grant programs.

REFERENCES

[1] Ziu, E., Khan, S. M. Z., and Mesfin, F. B., 2024. "Subarachnoid hemorrhage". [Updated 2023 Jun 1]. In: StatPearls [Internet]. Treasure Island (FL): StatPearls Publishing; 2024 Jan-. Available from: https://www.ncbi.nlm.nih.gov/books/NBK441958/.

[2] Van Gijn, J., Kerr, R. S., and Rinkel, G. J., 2007. "Subarachnoid haemorrhage". *The Lancet,* ***369***(9558), pp. 306–318.

[3] Bai, H.-z., Masuda, J., Sawa, Y., Nakano, S., Shirakura, R., Shimazaki, Y., Ogata, J., and Matsuda, H., 1994. "Neointima formation after vascular stent implantation. spatial and chronological distribution of smooth muscle cell proliferation and phenotypic modulation.". *Arteriosclerosis and thrombosis: a journal of vascular biology,* ***14***(11), pp. 1846–1853.

[4] Edelman, E. R., and Rogers, C., 1998. "Pathobiologic responses to stenting". *The American journal of cardiology,* ***81***(7), pp. 4E–6E.

[5] Palmaz, J. C., 1993. "Intravascular stents: tissue-stent interactions and design considerations.". *AJR. American journal of roentgenology,* ***160***(3), pp. 613–618.

[6] Virmani, R., and Farb, A., 1999. "Pathology of in-stent restenosis". *Current opinion in lipidology,* ***10***(6), pp. 499–506.

[7] Brisman, J. L., Song, J. K., and Newell, D. W., 2006. "Cerebral aneurysms". *New England journal of medicine,* ***355***(9), pp. 928–939.

[8] HospiMedica International staff writers, S., 2018. Flow diverting stent helps contain cerebrovascular defects. 24,Jul,2018.

[9] Jin, J., Guo, G., Ren, Y., Yang, B., Wu, Y., Wang, S., Sun, Y., Wang, X., Wang, Y., and Zheng, J., 2022. "Risk factors for recurrence of intracranial aneurysm after coil embolization: a meta-analysis". *Frontiers in Neurology,* ***13***, p. 869880.

[10] Bhogal, P., Udani, S., Cognard, C., Piotin, M., Brouwer, P., Sourour, N.-A., Andersson, T., Makalanda, L., Wong, K., Fiorella, D., et al., 2019. "Endosaccular flow disruption: where are we now?". *Journal of NeuroInterventional Surgery,* ***11***(10), pp. 1024–1025.

[11] Ries, T., Siemonsen, S., Thomalla, G., Grzyska, U., Zeumer, H., and Fiehler, J., 2007. "Long-term follow-up of cerebral aneurysms after endovascular therapy–prediction and outcome of retreatment". *American Journal of Neuroradiology,* ***28***(9), pp. 1755–1761.

[12] Romero Bhathal, J., Chassagne, F., Marsh, L., Levitt, M. R., Geindreau, C., and Aliseda, A., 2023. "Modeling flow in cerebral aneurysm after coils embolization treatment: a realistic patient-specific porous model approach". *Cardiovascular Engineering and Technology,* ***14***(1), pp. 115–128.

[13] Chen, C.-J., Dabhi, N., Snyder, M. H., Ironside, N., Abecassis, I. J., Kellogg, R. T., Park, M. S., and Ding, D., 2021. "Intrasaccular flow disruption for brain aneurysms: a systematic review of long-term outcomes". *Journal of Neurosurgery,* ***137***(2), pp. 360–372.

[14] Chung, B., and Cebral, J. R., 2015. "Cfd for evaluation and treatment planning of aneurysms: review of proposed clinical uses and their challenges". *Annals of biomedical engineering,* ***43***, pp. 122–138.

[15] Steinman, D. A., Milner, J. S., Norley, C. J., Lownie, S. P., and Holdsworth, D. W., 2003. "Image-based computational simulation of flow dynamics in a giant intracranial aneurysm". *American Journal of Neuroradiology,* ***24***(4), pp. 559–566.

[16] Xiang, J., Natarajan, S. K., Tremmel, M., Ma, D., Mocco, J., Hopkins, L. N., Siddiqui, A. H., Levy, E. I., and Meng, H., 2011. "Hemodynamic–morphologic discriminants for intracranial aneurysm rupture". *Stroke,* ***42***(1), pp. 144–152.

[17] Augsburger, L., Reymond, P., Rufenacht, D., and Stergiopulos, N., 2011. "Intracranial stents being modeled as a porous medium: flow simulation in stented cerebral aneurysms". *Annals of biomedical engineering,* ***39***, pp. 850–863.

[18] Jeong, W., Han, M. H., and Rhee, K., 2013. "Effects of framing coil shape, orientation, and thickness on intraaneurysmal flow". *Medical & biological engineering & computing,* ***51***, pp. 981–990.

[19] Malek, A. M., Higashida, R. T., Phatouros, C. C., Dowd, C. F., and Halbach, V. V., 1999. "Treatment of an intracranial aneurysm using a new three-dimensional-shape guglielmi detachable coil: technical case report". *Neurosurgery,* ***44***(5), pp. 1142–1144.

[20] Mehra, M., Hurley, M. C., Gounis, M. J., King, R. M., Shaibani, A., Dabus, G., Labdag, F. E., Levy, E. I., and Bendok, B. R., 2011. "The impact of coil shape design on angiographic occlusion, packing density and coil mass uniformity in aneurysm embolization: an in vitro study". *Journal of neurointerventional surgery,* ***3***(2), pp. 131–136.

[21] Bendsøe, M. P., and Kikuchi, N., 1988. "Generating optimal topologies in structural design using a homogenization method". *Computer methods in applied mechanics and engineering,* ***71***(2), pp. 197–224.

[22] Bendsøe, M. P., 1989. "Optimal shape design as a material distribution problem". *Structural optimization,* ***1***, pp. 193–202.

[23] Zhou, M., and Rozvany, G. I., 1991. "The coc algorithm, part ii: Topological, geometrical and generalized shape optimization". *Computer methods in applied mechanics and engineering,* ***89***(1-3), pp. 309–336.

[24] Mlejnek, H., 1992. "Some aspects of the genesis of structures". *Structural optimization,* ***5***, pp. 64–69.

[25] Allaire, G., Jouve, F., and Toader, A.-M., 2004. "Structural optimization using sensitivity analysis and a level-set method". *Journal of computational physics,* ***194***(1), pp. 363–393.

[26] Wang, M. Y., Wang, X., and Guo, D., 2003. "A level set method for structural topology optimization". *Computer methods in applied mechanics and engineering,* ***192***(1-2), pp. 227–246.

[27] Xie, Y. M., and Steven, G. P., 1993. "A simple evolutionary procedure for structural optimization". *Computers & structures,* ***49***(5), pp. 885–896.

[28] Duan, X., Ma, Y., and Zhang, R., 2008. "Optimal shape control of fluid flow using variational level set method". *Physics letters A,* ***372***(9), pp. 1374–1379.

[29] Duan, X.-B., Ma, Y.-C., and Zhang, R., 2008. "Shape-topology optimization for navier–stokes problem using variational level set method". *Journal of computational and applied mathematics,* ***222***(2), pp. 487–499.

[30] Duan, X.-B., Ma, Y.-C., and Zhang, R., 2008. "Shape-topology optimization of stokes flow via variational level set method". *Applied Mathematics and Computation,* ***202***(1), pp. 200–209.

[31] Zhang, B., and Liu, X., 2015. "Topology optimization study of arterial bypass configurations using the level set method". *Structural and Multidisciplinary Optimization,* ***51***, pp. 773–798.

[32] Bendsøe, M. P., and Sigmund, O., 1999. "Material interpolation schemes in topology optimization". *Archive of applied mechanics,* ***69***, pp. 635–654.

[33] Borrvall, T., and Petersson, J., 2003. "Topology optimization of fluids in stokes flow". *International journal for numerical methods in fluids,* ***41***(1), pp. 77–107.

[34] James, K. A., and Waisman, H., 2016. "Layout design of a bi-stable cardiovascular stent using topology optimization". *Computer Methods in Applied Mechanics and Engineering,* ***305***, pp. 869–890.

[35] Zhuang, R., Tian, J., Tassiopoulos, A., Sadasivan, C., Gu, X. D., and Chen, S., 2023. "Designing programmable ferromagnetic soft metastructures for minimally invasive endovascular therapy". In International Design Engineering Technical Conferences and Computers and Information in Engineering Conference, Vol. 87318, American Society of Mechanical Engineers, p. V03BT03A054.

[36] Ford, M. D., Stuhne, G. R., Nikolov, H. N., Habets, D. F., Lownie, S. P., Holdsworth, D. W., and Steinman, D. A., 2005. "Virtual angiography for visualization and validation of computational models of aneurysm hemodynamics". *IEEE transactions on medical imaging,* ***24***(12), pp. 1586–1592.

[37] Rayz, V. L., Boussel, L., Acevedo-Bolton, G., Martin, A. J., Young, W. L., Lawton, M. T., Higashida, R., and Saloner, D., 2008. "Numerical simulations of flow in cerebral aneurysms: comparison of cfd results and in vivo mri measurements".

[38] Hoi, Y., Woodward, S. H., Kim, M., Taulbee, D. B., and Meng, H., 2006. "Validation of cfd simulations of cerebral aneurysms with implication of geometric variations".

[39] Karmonik, C., Chintalapani, G., Redel, T., Zhang, Y. J., Diaz, O., Klucznik, R., and Grossman, R. G., 2013. "Hemodynamics at the ostium of cerebral aneurysms with relation to post-treatment changes by a virtual flow diverter: a computational fluid dynamics study". In 2013 35th Annual International Conference of the IEEE Engineering in Medicine and Biology Society (EMBC), IEEE, pp. 1895–1898.

[40] Jiang, Y., Ge, L., Di, R., Lu, G., Huang, L., Li, G., Leng, X., Zhang, S., Wan, H., Geng, D., et al., 2019. "Differences in hemodynamic characteristics under high packing density between the porous media model and finite element analysis in computational fluid dynamics of intracranial aneurysm virtual treatment". *Journal of neurointerventional surgery,* ***11***(8), pp. 853–858.

[41] Xiang, J., Damiano, R. J., Lin, N., Snyder, K. V., Siddiqui, A. H., Levy, E. I., and Meng, H., 2015. "High-fidelity virtual stenting: modeling of flow diverter deployment for hemodynamic characterization of complex intracranial aneurysms". *Journal of neurosurgery,* ***123***(4), pp. 832–840.

[42] Morales, H. G., Kim, M., Vivas, E., Villa-Uriol, M.-C., Larrabide, I., Sola, T., Guimaraens, L., and Frangi, A., 2011. "How do coil configuration and packing density influence intra-aneurysmal hemodynamics?". *American Journal of Neuroradiology,* ***32***(10), pp. 1935–1941.

[43] Morales, H. G., Larrabide, I., Geers, A. J., San Román, L., Blasco, J., Macho, J. M., and Frangi, A. F., 2012. "A virtual coiling technique for image-based aneurysm models by dynamic path planning". *IEEE transactions on medical imaging,* ***32***(1), pp. 119–129.

[44] Jiang, L., Chen, S., Sadasivan, C., and Jiao, X., 2017. "Structural topology optimization for generative design of personalized aneurysm implants: Design, additive manufacturing, and experimental validation". In 2017 IEEE Healthcare Innovations and Point of Care Technologies (HI-POCT), IEEE, pp. 9–13.

[45] Sá, L., Romero, J., Horikawa, O., and Silva, E. C. N., 2018. "Topology optimization applied to the development of small scale pump". *Structural and Multidisciplinary Optimization,* ***57***, pp. 2045–2059.

[46] Kumar, P., Frouws, J. S., and Langelaar, M., 2020. "Topology optimization of fluidic pressure-loaded structures and compliant mechanisms using the darcy method". *Structural and Multidisciplinary Optimization,* ***61***, pp. 1637–1655.

[47] Wu, J., Aage, N., Westermann, R., and Sigmund, O., 2018. "Infill optimization for additive manufactur-

ing—approaching bone-like porous structures". *IEEE Transactions on Visualization and Computer Graphics,* ***24***(2), pp. 1127–1140.

[48] Damiano, R. J., Tutino, V. M., Paliwal, N., Patel, T. R., Waqas, M., Levy, E. I., Davies, J. M., Siddiqui, A. H., and Meng, H., 2020. "Aneurysm characteristics, coil packing, and post-coiling hemodynamics affect long-term treatment outcome". *Journal of NeuroInterventional Surgery,* ***12***(7), pp. 706–713.

[49] Ye, Q., Guo, Y., Chen, S., Lei, N., and Gu, X. D., 2019. "Topology optimization of conformal structures on manifolds using extended level set methods (x-lsm) and conformal geometry theory". *Computer Methods in Applied Mechanics and Engineering,* ***344***, pp. 164–185.

[50] Xu, X., Gu, X. D., and Chen, S., 2022. "Shape and topology optimization of conformal thermal control structures on free-form surfaces: A dimension reduction level set method (dr-lsm)". *Computer Methods in Applied Mechanics and Engineering,* ***398***, p. 115183.

[51] Tian, J., Li, M., Han, Z., Chen, Y., Gu, X. D., Ge, Q., and Chen, S., 2022. "Conformal topology optimization of multi-material ferromagnetic soft active structures using an extended level set method". *Computer Methods in Applied Mechanics and Engineering,* ***389***, p. 114394.